Magnetic properties of transition-metal-doped $Zn_{1-x}T_xO$ (T=Cr, Mn, Fe, Co, and Ni) thin films with and without intrinsic defects: A density functional study

Qian Wang,[1,2,*] Qiang Sun,[3,4] Puru Jena,[2] and Y. Kawazoe[5]

[1]*School of Physical Science and Technology, Southwest University, Chongqing 400715, China*
[2]*Department of Physics, Virginia Commonwealth University, Richmond, Virginia 23284, USA*
[3]*Department of Advanced Materials and Nanotechnology, Peking University, Beijing, China*
[4]*Center for Applied Physics and Technology, Peking University, Beijing 100871, China*
[5]*Institute for Materials Research, Tohoku University, Sendai 980-8577, Japan*

Theoretical calculations based on density-functional theory and generalized gradient approximation have been carried out in studying the electronic structure and magnetic properties of transition-metal-doped $Zn_{1-x}T_xO$ (T=Cr, Mn, Fe, Co, and Ni) $(11\bar{2}0)$ thin films systematically with and without intrinsic point defects (e.g., vacancies and interstitials), and as function of concentration and distribution of dopants and vacancies. Using large supercells and geometry optimization without symmetry constraint, we are able to determine the sites that metal atoms prefer to occupy, their tendency to cluster, the preferred magnetic coupling between magnetic moments at transition-metal sites, and the effect of intrinsic point defects on the nature of their coupling. Except for Mn atom, which distributes uniformly in ZnO thin films in dilute condition, transition-metal atoms occupying Zn sites prefer to reside on the surface and couple antiferromagnetically. The presence of native point defects has a large effect on the ground-state magnetic structure. In particular, p-type defects such as Zn vacancies play a crucial role in tuning and stabilizing ferromagnetism in $Zn_{1-x}T_xO$ thin films (T=Cr, Mn, Fe, and Ni), while n-type defects such as O vacancies or Zn interstitials greatly enhance the ferromagnetic coupling in $Zn_{1-x}Co_xO$ thin films. The present study provides a clear insight into the numerous conflicting experimental results on the magnetic properties of T-doped ZnO systems.

I. INTRODUCTION

Spintronics is a relatively new research field where the manipulations of the electron spin as well its charge can give rise to new devices. For this reason, it is essential to develop semiconductors with ferromagnetically polarized carriers at room temperature so that the spin as well as charge of the carriers can be coupled with an external magnetic field. Recently ZnO-based materials have received considerable attention. This is due to the electrical, optical, and acoustic properties of the host semiconductor ZnO, and the theoretical prediction[1] and experimental reports of room-temperature ferromagnetism (FM).[2–5] Unfortunately, there has been considerable controversy in reported experimental results. For example, some authors have found Fe-ZnO,[6,7] Co-ZnO,[8–10] Ni-ZnO,[11] Cr-ZnO,[12,13] and Mn-ZnO (Refs. 14 and 15) to be paramagnetic (PM) or antiferromagnetic (AFM) while others reported ferromagnetism in some samples of ZnO containing Ti, V, Cr, Mn, Fe, Co, or Ni.[2–5,16–21]

It is natural to suggest that ferromagnetism is merely due to magnetic impurities such as Cr, Mn, Fe, Co, and Ni but some experimental results appear to rule this out.[6–15] Presently, there is no consensus on the microscopic mechanism responsible for ferromagnetism in ZnO-based DMSs although several have been proposed for the bulk system, for example, carrier-induced ferromagnetism[1,22–24] and percolation of bound magnetic polarons.[25,26] To the best of our knowledge, no theoretical work exists on (Zn, T)O (T=Fe, Co, and Ni) thin-film systems. The reason for this is the difficulty of thin-film calculations because of the complicated surface reconstruction and the large supercells that

are needed for modeling the low doping concentration (∼3%–15%) encountered in experiments. We have studied the magnetic coupling between Mn atoms in (Zn, Mn)O thin films,[23,27] Cr atoms in (Zn, Cr)O $(10\bar{1}0)$ thin films,[28] and V atoms in (Zn, V)O $(11\bar{2}0)$ thin films.[29]

We note that in the bulk phase Cr, Mn, Fe, Co, and Ni have different crystal structures and magnetic properties. How different are their magnetic properties when doped in ZnO thin films? Why do experimental results differ so much? To answer these questions, we have carried out a comprehensive first-principles theoretical investigations of energetics, electronic structure, and magnetic properties of T-doped ZnO thin films (T=Cr, Mn, Fe, Co, and Ni) having wurtzite structure and $[11\bar{2}0]$ orientation. Additionally, we have studied the effect of native defects (vacancies and interstitials) on their electronic and magnetic properties. We primarily focus on three problems: (1) for a given concentration and no defects, what are the preferred sites and magnetic coupling between Cr, Mn, Fe, Co, and Ni atoms in ZnO thin films? (2) How do these properties depend on the dopant concentration? (3) What role do native point defects such as vacancies and interstitials have on the preferred magnetic coupling in $Zn_{1-x}T_xO$ thin films?

II. COMPUTATIONAL PRODEDURE

Calculations are carried out using density-functional theory[30] (DFT) that incorporates exchange and correlation effects within the generalized gradient approximation (GGA).[31] The analysis of electronic structure and magnetic
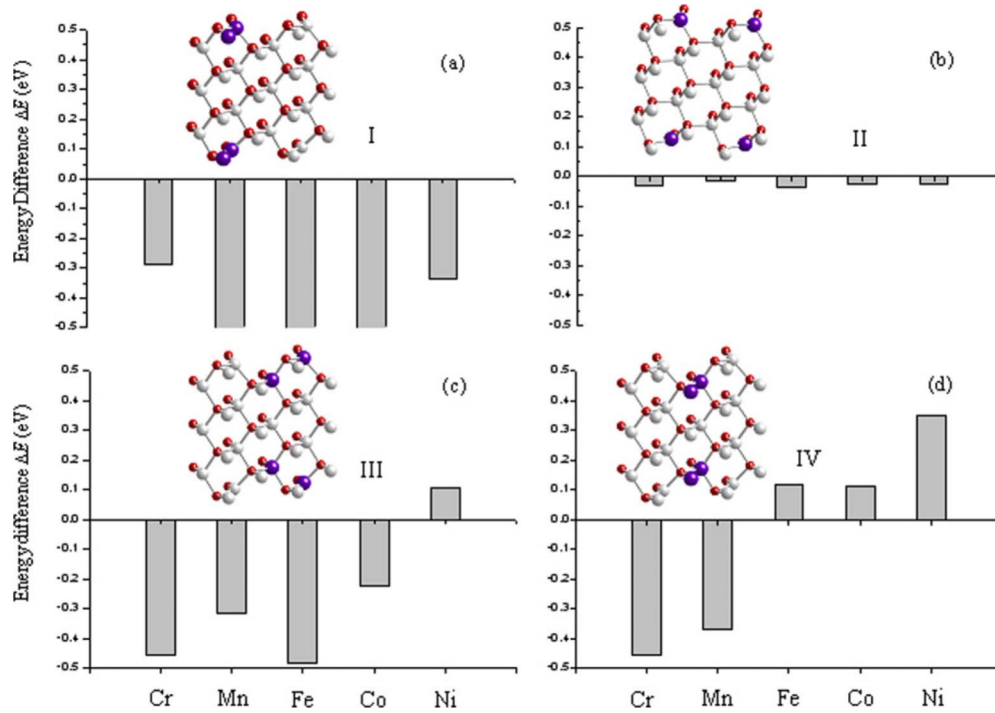
FIG. 1. (Color online) Energy differences, $\Delta E = E_{AFM} - E_{FM}$, for four configurations of the seven-layer slab supercell $Zn_{0.857}T_{0.143}O$ (T=Cr, Mn, Fe, Co, and Ni). The light gray (lighter) spheres are Zn, the red (darker) spheres are O, and the purple (bigger) spheres are TM atoms.

properties are performed using PW91 functional for GGA and a plane-wave basis set with the projector augmented wave (PAW) method[32] as implemented in the Vienna *Ab initio* Simulation Package (VASP).[33] The cutoff energy was set at 320 eV for the plane-wave basis (the default of maximum cutoff energy is 276.75 eV). Self-consistency has been achieved by allowing the total energy to converge within 1 meV because of the very small energy difference expected between the FM and AFM states. Hellman-Feynman force components on each ion in the supercells are converged to 1 meV/Å.

Pure ZnO normally crystallizes in the hexagonal wurtzite structure, which consists of Zn and O planes stacked alternatively along the c axis, and the Zn and O ions are tetrahedrally coordinated. ZnO can be transformed into the cubic rocksalt (NaCl) structure by the application of high pressure. The lattice constants are $a=b=3.249$ Å, and $c=5.205$ Å, with a space-group $P6_3mc$ (No. 186).[34] ZnO thin film was modeled by a (1×2) seven-layer slab having $[11\bar{2}0]$ surface orientation, as shown in Fig. 1, containing 28 formula units ($Zn_{28}O_{28}$). Each slab was separated from the other by a vacuum region of 10 Å along the $[11\bar{2}0]$ direction. The central three layers of the slab were held at their bulk position while the two layers on either side of the slab were taken to be identical to preserve symmetry and were allowed to relax without further symmetry constraint. To study the magnetic coupling between T atoms, we replaced a pair of Zn atoms with two T (T=Cr, Fe, Co, and Ni) atoms of the same type on the top and bottom of the seven-layer slab ($Zn_{28}O_{28}$). This yields a T dopant concentration of 14.28%. In each case we explored four configurations where T atoms replaced Zn sites

(see Fig. 1). The geometry optimization and total-energy calculations were carried out corresponding to both FM and AFM spin alignments to determine the lowest energy configuration, and hence the preferred geometrical and magnetic states. The magnetic moments located on each T atom and the *spd* site projected wave-function characters have been calculated self-consistently for all the configurations. To study the effect of dopant concentration on the magnetic coupling, we increased the slab thickness along the $[11\bar{2}0]$ direction as well as the $[1\bar{1}00]$ direction. Calculations were carried out for (1×2) nine-layer and 11-layer slab supercells, and (2×2) seven-layer slab supercell corresponding, respectively, to 11.11%, 9.10%, and 7.14% T dopant concentration. For the (1×2) slab supercells we used $(6 \times 4 \times 1)$ and $(8 \times 6 \times 1)$ Monkhorst-Pack grid,[35] respectively, for the structure optimization and for total-energy and charge-density calculations, while for the (2×2) supercell, $(5 \times 5 \times 1)$ and $(7 \times 7 \times 1)$ grids were selected. The local magnetic moments at T atoms as well as the partial density of states (DOS) were calculated within the Wigner-Seitz radius: 1.323, 1.323, 1.302, 1.302, 1.286, 1.270, and 0.820 Å for Cr, Mn, Fe, Co, Ni, Zn, and O, respectively, which are chosen based on PW91 potentials implemented in the VASP code. We have verified that the thickness of the slab and the vacuum space are adequate to simulate the thin films.[27] The surface reconstruction and the reliability of our calculations have been well established in our previous work.[27–29] The calculated lattice parameters, $a=b=3.262$ Å and $c=5.226$ Å agree well with the available experimental data of 3.249 and 5.205 Å, respectively. For the dimers, Cr_2, Mn_2, Fe_2, Co_2, and Ni_2, the ground states are, respectively, found to be $^1\Sigma_g^+$,

TABLE I. Energy difference ΔE between AFM and FM states ($\Delta E = E_{AFM} - E_{FM}$, in eV/supercell), relative energy $\Delta\varepsilon$ (in eV) calculated with respect to the ground-state configuration I, optimized T-T distance $d_{T\text{-}T}$ (in Å), and magnetic moments (in μ_B) at each T atom for all the configurations given in Fig. 1 for $Zn_{24}T_4O_{28}$ thin-film supercell (T=Cr, Mn, Fe, Co, and Ni).

Configs.	ΔE	$\Delta\varepsilon$	$d_{T\text{-}T}$	μ_{T1}	μ_{T2}
			T=Cr		
I	−0.287	0.000	2.848	2.959	−2.962
II	−0.032	0.547	5.638	3.205	−3.202
III	−0.454	0.883	2.907	2.635	−2.798
IV	−0.450	1.810	3.098	2.682	−2.922
			T=Mn		
I	−0.830	0.000	2.909	4.166	−4.127
II	−0.014	0.721	5.62	4.218	−4.216
III	−0.312	0.553	3.21	4.178	−4.142
IV	−0.369	0.679	3.17	4.158	−4.150
			T=Fe		
I	−0.919	0.000	2.888	3.236	−3.237
II	−0.017	0.771	5.628	3.472	−3.470
III	−0.482	1.285	2.916	3.372	−3.539
IV	0.115	1.917	3.205	3.574	3.580
			T=Co		
I	−0.495	0.000	2.865	2.123	−2.119
II	0.006	0.703	5.629	2.433	−2.434
III	−0.190	0.779	2.963	2.298	−2.329
IV	0.112	1.293	3.165	2.335	2.337
			T=Ni		
I	−0.332	0.000	2.885	1.039	−1.039
II	−0.013	0.692	5.628	1.430	−1.431
III	0.108	1.459	2.945	1.496	1.527
IV	0.350	2.268	3.123	1.513	1.515

$^{11}\Pi_u$, $^{7}\Delta_u$, $^{5}\Delta_g$, and $^{3}\Sigma_g^-$ with bond lengths of 1.78, 2.56, 1.99, 1.98, and 2.02 Å, in good agreement with experiment.[36]

III. RESULTS AND DISCUSSIONS

A. Site preference of T atoms

First, we determined the preferred site of the T atoms in a $ZnO(11\bar{2}0)$ thin film. This is achieved by substituting a *single* Zn atom with a T (T=Cr, Fe, Co, and Ni) atom at a surface site and then at a subsurface site. To preserve symmetry, we also replaced the corresponding Zn atoms on the bottom surface and subsurface layers. This led to a T concentration of 7.14%. As the two T atoms on the top and bottom of the slab are far enough to not interact with each other, the surpercell geometry of $Zn_{0.929}T_{0.071}O$ gives us in-

formation on the site preference of T atoms in the dilute regime. The geometry optimization for each doping configuration was carried out using a $(6 \times 4 \times 1)$ Monkhorst-Pack k-point grid. It was found that the total energy of the slab with a T (T=Cr, Fe, Co, and Ni) replacing Zn at surface sites is 0.826, 0.702, 0.281, and 1.113 eV lower in energy than that with a T substituting the subsurface Zn sites, respectively. This indicates that Cr, Fe, Co, and Ni prefer to reside on the surface, similar to what had been found in Cr-doped $ZnO(10\bar{1}0)$ thin films[28] and Cr-doped GaN thin films.[37] Mn, on the other hand, exhibits no site preference as the calculated energy difference between the surface and subsurface site is only 0.07 eV. Thus, Mn can be distributed uniformly in ZnO thin films[27] in the dilute regime. The possible reason for this difference in site preference between Mn and other dopants is that Mn, with a half-filled 3d and filled 4s shell
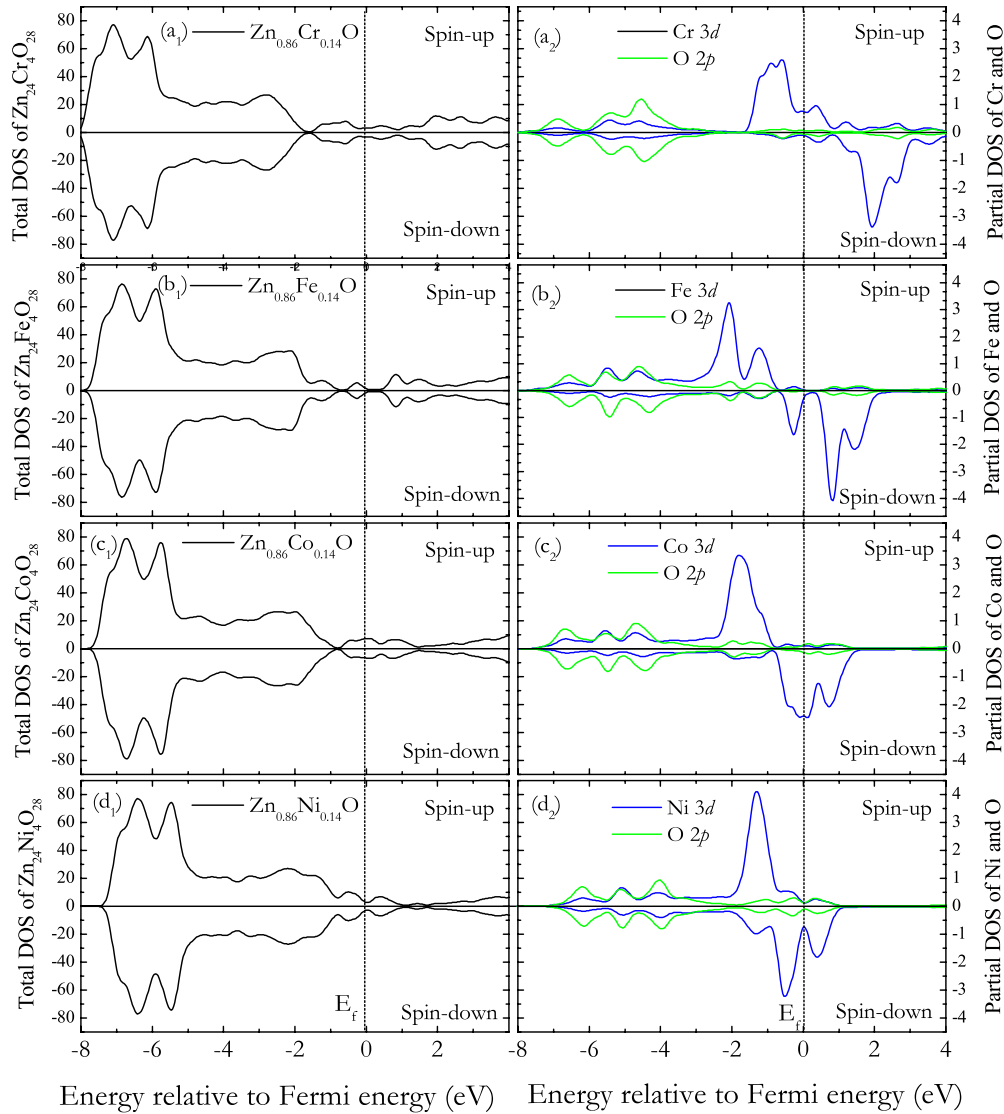
FIG. 2. (Color online) [(a_1)–(d_1)] Total spin DOS, and [(a_2)–(d_2)] partial spin DOS of T $3d$ and O $2p$ in $Zn_{24}T_4O_{28}$ (T=Cr, Fe, Co, and Ni).

$(3d^54s^2)$, interacts weakly with neighboring atoms. This can be seen by measuring the average distance between the dopant atom and neighboring oxygen which are 1.935, 1.892, 1.881, 1.856, and 1.853 Å for Mn, Cr, Fe, Co, and Ni atoms, respectively, and comparing with the corresponding distance of 1.920 Å between Zn and O. In addition, Mn can have multiple valence states ranging from +2 to +7, which makes the bonding of Mn with the substrate more flexible than for other transition-metal atoms. The magnetic moments on Cr, Fe, Co, and Ni atoms are, respectively, $3.105\mu_B$, $3.490\mu_B$, $2.443\mu_B$, and $1.436\mu_B$, and mainly arise from their $3d$ orbitals ($3.00\mu_B$, $3.42\mu_B$, $2.39\mu_B$, and $1.39\mu_B$) with negligible contributions from $4s$ ($0.07\mu_B$, $0.01\mu_B$, $0.01\mu_B$, and $0.01\mu_B$) and $3p$ orbitals ($0.03\mu_B$, $0.06\mu_B$, $0.05\mu_B$, and $0.04\mu_B$). The hybridization between T $3d$ and its neighboring O $2p$ orbitals reduces the magnetic moment as compared to that of a free T atom. The induced magnetic moment in the nearest-neighbor (NN) O p orbitals are $-0.027\mu_B$, $-0.145\mu_B$, $-0.178\mu_B$, $-0.151\mu_B$ for Cr, Fe, Co, and Ni, respectively.

B. Magnetic coupling between T atoms without presence of any native defects

We now discuss the magnetic coupling between a pair of T atoms in $ZnO(11\bar{2}0)$ thin films. To this end, we substituted two Zn atoms with two T (T=Cr, Fe, Co, and Ni) atoms of one type, each time on both the top and bottom sides of the $Zn_{28}N_{28}$ slab. This yields a dopant concentration of 14.28% and a $Zn_{0.857}M_{0.143}O$ slab supercell. The four configurations (in Fig. 1) are designed to study the dependence of magnetic exchange interaction between the dopants sites on separation distance. Configuration I corresponds to replacing two Zn atoms with T at the nearest-neighbor sites on the surface layer of the slab. Configuration II represents the replacement of two Zn atoms with T at surface sites with further separation distance. Configuration III is achieved by replacing two Zn atoms with T atoms at the nearest-neighbor sites with one Zn atom on the surface layer and the other on the second layer. Configuration IV corresponds to replacing two nearest

TABLE II. Composition of Co-doped ZnO slab, Co concentration x (at. %), total-energy difference between the AFM and FM states ($\Delta E = E_{AFM} - E_{FM}$, in eV) for two Co atoms at the nearest-neighbor surface Zn sites (ΔE_{NN}) and when separated by a far distance (ΔE_{FS}), relative energy $\Delta \varepsilon$ (in eV) calculated with respect to the ground-state configuration NN, optimized average Zn-O and Co-O bond lengths (d_{Zn-O} and d_{Co-O}, respectively, in Å) on the surface and Co-Co distance (d_{Co-Co}, in Å), and magnetic moment (in μ_B) on each Co atom for the supercells listed in the first column.

Supercells	Slab layers	x (at. %)	ΔE_{NN}	ΔE_{FS}	$\Delta \varepsilon$	d_{Zn-O}	d_{Co-O}	d_{Co-Co}	μ_{Co1}	μ_{Co2}
$Zn_{52}Co_4O_{56}$	$(2 \times 2) - 7L$	7.14	−0.098	0.004	0.356	1.892	1.820	2.852	2.309	−2.299
$Zn_{40}Co_4O_{44}$	$(1 \times 2) - 11L$	9.10	−0.479	0.007	0.687	1.889	1.811	2.901	2.119	−2.115
$Zn_{32}Co_4O_{36}$	$(1 \times 2) - 9L$	11.11	−0.485	0.009	0.692	1.889	1.809	2.895	2.112	−2.113
$Zn_{24}Co_4O_{28}$	$(1 \times 2) - 7L$	14.29	−0.509	0.006	0.703	1.890	1.808	2.875	2.123	−2.119

Zn atoms on the second layer. The preferred magnetic coupling between the T atoms is determined by allowing them to couple both ferromagnetically and antiferromagnetically, and comparing their total energies and calculating $\Delta E = E_{AFM} - E_{FM}$. Positive ΔE means that the FM state is lower in energy than the AFM state. The calculated ΔE's are plotted in Fig. 1 [for comparison, the results for $T = Mn$ (Ref. 27) is also included]. The relative energies of the remaining three configurations (II–IV) $\Delta \varepsilon$, measured with respect to the ground-state configuration for each element, $T = Cr$, Mn, Fe, Co, and Ni, are also plotted in Fig. 1. The magnetic moments on each of the T atoms for all the configurations are calculated and summarized in Table I.

We see that configuration I, where the two T atoms are at the nearest-neighbor sites on the surface, is the ground state of Cr-doped, Mn-doped, Fe-doped, Co-doped, and Ni-doped ZnO. The corresponding magnetic couplings are AFM that lie 0.287, 0.830, 0.919, 0.495, and 0.332 eV/supercell lower in energy than the FM state for Cr, Mn, Fe, Co, and Ni, respectively. We also note that the total-energy difference between FM and AFM states is reduced to 0.006–0.032 eV when the distance between two T atoms are increased to about 5.60 Å away from each other [see configuration II in Fig. 1(b)]. This suggests that the AFM interaction is short ranged in T-doped ZnO thin films. The relative energy $\Delta \varepsilon$ markedly increases when the distance between the T site increases or the T atoms move from the surface sites to subsurface sites of the slab. Therefore, it is clear that the AFM coupled states are energetically favorable for T atoms in $Zn_{0.857}T_{0.143}O$ ($T = Cr$, Mn, Fe, Co, and Ni) thin films, and Cr, Co, Fe, and Ni atoms prefer to occupy the surface sites and cluster around the neighboring O atom.

In the ground-state configuration, the calculated T-T distance is 2.848, 2.909, 2.888, 2.865, and 2.885 Å for $T = Cr$, Mn, Fe, Co, and Ni, respectively, leading to a contraction of −4.14%, −2.09%, −2.79%, −4.71%, and −2.89% as compared to those in bulk. The Cr, Mn, Fe, Co, and Ni atoms carry an average magnetic moment of $2.959\mu_B$, $4.166\mu_B$, $3.236\mu_B$, $2.123\mu_B$, and $1.039\mu_B$, respectively. The corresponding p orbitals of nearest-neighbor O atom are polarized with each carrying a moment of $0.058\mu_B$, $0.093\mu_B$, $0.199\mu_B$, $0.208\mu_B$, and $0.186\mu_B$.

The total DOS for spin-up and spin-down electrons for the ground-state configurations of T-doped ZnO are shown in Figs. 2(a$_1$)–2(d$_1$). The corresponding partial spin DOS of the T 3d orbitals and its neighboring O 2p orbitals are shown in Figs. 2(a$_2$)–2(d$_2$). From the total DOSs, we see that doping of a T into a ZnO thin film has introduced new states in the energy-gap region of the pure ZnO thin film but the DOSs for spin-up and spin-down states are identical leading to zero magnetic moment. This is to be expected in an AFM system. Meanwhile, Figs. 2(a$_2$)–2(d$_2$) show that T 3d levels dominate the DOS at the Fermi energy and overlap with O 2p states. This indicates that there is a strong interaction between T and the neighboring O atoms, which results in the opposite magnetic moments of O atoms. The contribution to the moment coming from T 3d orbitals is $2.859\mu_B$, $3.930\mu_B$, $3.189\mu_B$, $2.095\mu_B$, and $1.015\mu_B$ for $T = Mn$, Cr, Fe, Co, and N, respectively.

C. Effect of T dopant concentration on magnetic coupling

To study the effect of T concentration on the preferred magnetic coupling between the T atoms, we performed extensive calculations on $Zn_{1-x}T_xO$ thin films for different T doping concentrations by increasing the supercell thickness along the $[11\bar{2}0]$ direction, as well as along the $[1\bar{1}00]$ direction. At first, we carried out calculations for (1×2) nine-layer and 11-layer slab supercells for the $(Zn, T)O$ $(11\bar{2}0)$ thin-film surface. T dopant concentrations of 11.11% and 9.09% were achieved by substituting two Zn atoms with T on either side of the slabs. To determine the preferred geometrical and magnetic ground states, as well as to understand how the magnetic coupling between T atoms vary with the distance between them, we have constructed two configurations: when two T atoms substitute Zn at the NN sites on the surface layer [similar to configuration I in Fig. 1(a)], and when two T atoms are distributed with farther separation (FS) distance [similar to configuration II in Fig. 1(b)]. We did not consider configurations where Zn atoms on the subsurface layer are replaced by T because the total energy of the supercells is higher by 0.553–2.268 eV than that for T atoms replacing Zn on the surface layer (see Table I). The calculations are carried out for Co dopant only to demonstrate the effect of concentration. The calculated results are summarized in Table II. We note that the Zn-O and Co-O bond lengths on the surface layer for the (1×2) slabs converged in the seven-layer slab.

We found that configuration NN is the ground-state geometry with the AFM state lying 0.485 and 0.479 eV/supercell
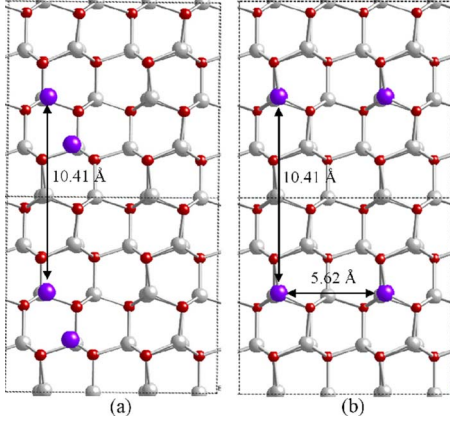
FIG. 3. (Color online) Top view of the two optimized adjacent seven-layer slab supercells ($Zn_{52}Co_4O_{56}$) along the $[1\bar{1}00]$ direction with two Co atoms replacing Zn at (a) the NN and (b) the FS sites. The light gray (lighter) spheres are Zn, the red (darker) spheres are O, and the purple (bigger) spheres are Co.

lower in energy than the FM state, and configuration FS is 0.692 and 0.687 eV higher in energy than the ground state of configuration NN for the concentration of $x=11.11$ and 9.10 (at. %), respectively. These results are comparable with those for the concentration of $x=14.29\%$ (see Table II). In the ground-state configurations for the seven-layer to 11-layer supercells, the large values of energy difference ΔE show the stability of AFM coupling. However, the energy difference ΔE dramatically decreases with the increasing distance of Co separations. We note when two Co atoms are separated away by ~ 5.6 Å in configuration FS, the AFM and FM states are almost energetically degenerate. This suggests that the AFM interaction is short ranged in $Zn_{1-x}Co_xO$ thin films. The distribution of magnetic moments and DOS at the Fermi level show no significant change when compared with those for the seven-layer slab supercell.

We note that in all the (1×2) seven-layer to 11-layer slab supercell calculations above, T atoms in configuration NN may form a continuous zigzag chain along the $[1\bar{1}00]$ direction. One may wonder if the AFM coupling results from the formation of T-T chains, and if there is an interaction between the impurity atom and its image in the nearest supercell. We, therefore, repeated the calculations using a (2×2)

seven-layer ZnO $(11\bar{2}0)$ slab supercell $(Zn_{56}O_{56})$ by increasing the slab thickness along the $[1\bar{1}00]$ direction. In the (2×2) seven-layer supercell $(Zn_{56}O_{56})$, the minimum distance between the impurity atom and its image in the adjacent supercell is 10.41 Å along the $[1\bar{1}00]$ direction [see Fig. 3(a)]. In the calculations, the central three layers of this slab were fixed at the bulk crystalline position while the top and bottom two layers were relaxed without any symmetry constraint. When two T atoms are substitutionally doped at Zn sites on either side of the slab, a $Zn_{52}T_4O_{56}$ supercell with a concentration of 7.14% T is formed, which is closer to the concentration studied in most experiments, namely, $\sim 3\%$–15%. We have again selected the configurations NN and FS, as shown in Figs. 3(a) and 3(b), respectively, to search for the geometrical and magnetic ground states. The geometry optimization and total-energy calculations for the FM and AFM spin alignments were carried out for both NN and FS configurations for all of T (T=Cr, Mn, Fe, Co, and Ni) in $Zn_{0.929}T_{0.071}O$ supercells. The calculated results are tabulated in Tables II and III.

Our calculations once again indicate that the AFM coupling is preferable to the FM one and configuration NN has lower energy than configuration FS for all of the $Zn_{0.929}T_{0.071}O$ (T=Cr, Mn, Fe, Co, and Ni) supercells. In the ground-state configuration, the AFM state is found to be lower in energy by -0.094, -0.601, -0.832, -0.098, and -0.102 eV than the FM state for $Zn_{0.929}T_{0.071}O$ with T=Cr, Mn, Fe, Co, and Ni, respectively. Therefore, we verified that T-doped ZnO does not show FM behavior, as reported in the experiments.[6–15] The total magnetic moment for the $Zn_{0.929}T_{0.071}O$ supercell is found to be zero while the average local moment on each T atom is calculated to be $3.159\mu_B$, $3.884\mu_B$, $3.351\mu_B$, $2.304\mu_B$, and $1.283\mu_B$, respectively. The primary contribution to the magnetic moment comes from T $3d$ orbitals with small contributions from T $4s$ and T $3p$ due to sp and d hybridizations. The neighboring O atom is polarized antiferromagnetically with a magnetic moment of about $\sim 0.050\mu_B$–$0.175\mu_B$. The oxidation state of T ions is found to be T^{2+} in the $Zn_{1-x}T_xO$ thin films, which is isoelectronic with Zn (Zn^{2+}). Replacing Zn with T does not introduce any extra carriers to mediate the magnetic coupling. This would be the physical reason for the AFM coupling of T atoms in $Zn_{1-x}T_xO$.

Thus, it is clear that, in $Zn_{1-x}T_xO$ (T=Cr, Mn, Fe, Co, and Ni) thin films, AFM ordering is energetically favorable, rela-

TABLE III. Energy difference ΔE between AFM and FM states ($\Delta E = E_{AFM} - E_{FM}$), optimized T-T distance $d_{T\text{-}T}$, and the average magnetic moment μ_T at each T atom for the ground-state configuration of $Zn_{52}T_4O_{56}$ (T=Cr, Mn, Fe, Co, and Ni) supercell in the cases of defect-free, containing the oxygen vacancies (V_O) and the zinc vacancies (V_{Zn}).

Supercells	ΔE (eV/supercell)			$d_{T1\text{-}T2}$ (Å)			μ_T (μ_B)		
	Defect-free	V_O	V_{Zn}	Defect-free	V_O	V_{Zn}	Defect-free	V_O	V_{Zn}
$Zn_{52}Cr_4O_{56}$	-0.094	-0.149	0.089	2.875	2.486	3.147	3.159	3.128	2.810
$Zn_{52}Mn_4O_{56}$	-0.601	-0.688	0.065	2.561	2.541	3.534	3.884	3.993	3.479
$Zn_{52}Fe_4O_{56}$	-0.823	-0.094	0.887	2.818	2.409	3.493	3.351	3.239	3.216
$Zn_{52}Co_4O_{56}$	-0.098	0.683	-0.501	2.852	2.270	3.120	2.304	2.034	2.485
$Zn_{52}Ni_4O_{56}$	-0.102	-0.026	0.045	2.843	3.001	3.092	1.283	0.924	1.337

tive to the FM state, and the magnetic coupling between T atoms is insensitive to the concentration of T in the range of 7.14%–14.3%. Our results suggest that it is unlikely to achieve FM $Zn_{1-x}T_xO$ thin films without further modification, which is in agreement with recent experimental observations,[6–15] where the $Zn_{1-x}T_xO$ ($x=0.05\sim0.15$ at. %) thin films exhibited AFM or PM behavior. Therefore, the observed ferromagnetism must be associated with other factors, such as sample preparation conditions or intrinsic structural defects. In the following we explore this possibility.

D. Intrinsic defects cause ferromagnetism in $Zn_{1-x}T_xO$ thin films

Recently, a number of experiments have shown the correlation between the FM behavior and structural defects, such as Zn interstitials,[38–40] oxygen vacancies,[41–43] and/or Zn vacancies,[44–47] which indicate that defects play crucial roles in the observed FM behavior in ZnO-based DMSs. Concurrently, first-principles investigations of native point defects in bulk ZnO have been performed.[48,49] However, theoretical studies of the effect of defects on the magnetic properties of T-doped ZnO are few and conflicting. For example, Lee and Chang[50] found that, using the local spin-density approximation (LSDA), a sufficient supply of electron carriers is required to achieve ferromagnetism in bulk $Zn_{1-x}Co_xO$ while Spaldin[51] suggested that, based on pseudopotential calculations with localized atomic-orbital basis sets, ferromagnetism in bulk Co-doped or Mn-doped ZnO only occurs in the presence of simultaneous p doping (holes). No explanation exists to account for this discrepancy nor has any attempt been made to investigate the effect of defects on the magnetic coupling of T atoms in $Zn_{1-x}T_xO$ thin films. As mentioned before, these are plagued with numerous controversial experimental findings. We have, therefore, investigated the effect of oxygen vacancy (V_O), one of the most common n-type native defects, and zinc vacancy (V_{Zn}), one of the most common p-type defects, on the magnetism of $Zn_{1-x}T_xO$ (T=Cr, Mn, Fe, Co, and Ni,) thin films. We have also studied the influence of Zn (Zn_i) and O interstitials (O_i) on the electronic and magnetic properties of Co-doped ZnO

1. Oxygen vacancies

We chose the (2×2) seven-layer slab supercell ($Zn_{56}O_{56}$) to mimic the ZnO ($11\bar{2}0$) thin-film surface and started with the ground-state configuration of $Zn_{52}T_4O_{56}$ (T=Cr, Mn, Fe, Co, and Ni) to study how these defects influence the electronic and magnetic properties. First we created an oxygen vacancy V_O by removing a *single* O atom from the nearest-neighbor site of T atoms (forming-T-V_O-T-) on the surface layer of the slab [see Fig. 4(a)]. To preserve symmetry, the O atom on opposite side of the slab was also removed. This led to a $Zn_{52}T_4O_{54}$ supercell with V_O concentration of 3.6%. We calculated the electronic structure and magnetic coupling between T atoms in the presence of vacancies following the same procedure as performed for the defect-free $Zn_{0.929}T_{0.071}O$ systems. The calculated results are tabulated in Table III.
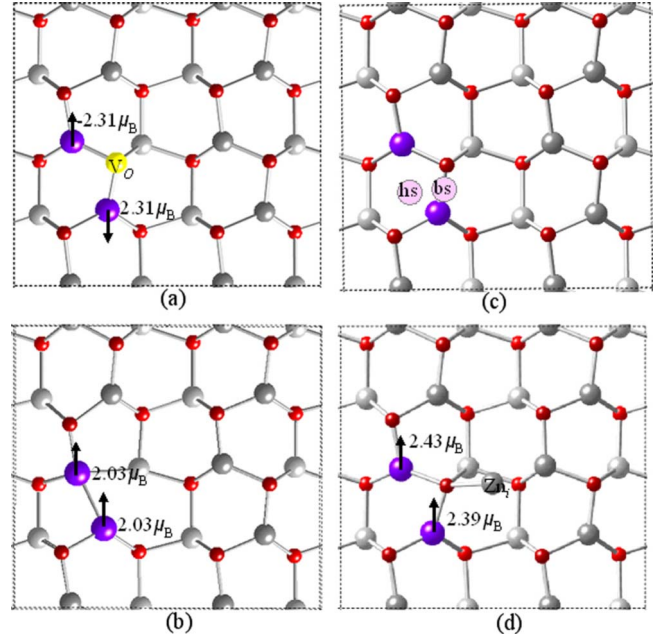

FIG. 4. (Color online) Top view of the topmost two layers of supercell $Zn_{52}Co_4O_{56}$ containing the defects. (a) Yellow sphere specifies the O site removed to generate V_O; (b) optimized geometry of the supercell in the presence of V_O; (c) two of the possible locations, hs and bs, for introducing O_i or Zn_i; (d) optimized geometry with the Zn_i. The light gray (lighter) spheres are Zn, the red (darker) spheres are O, and the purple (bigger) spheres are Co.

In the presence of V_O (electron carriers), it was found that AFM state is more favored than the FM one when the V_O is introduced in $Zn_{0.929}Cr_{0.071}O$ and $Zn_{0.929}Mn_{0.071}O$ supercells as the energy difference ΔE between the AFM and FM states decreased from -0.094 to -0.149 eV for $Zn_{0.929}Cr_{0.071}O$, and from -0.601 to -0.688 eV for $Zn_{0.929}Mn_{0.071}O$ supercells. However, the AFM coupling between Co atoms in $Zn_{0.929}Co_{0.071}O$ turns into FM with a large energy difference between the FM and AFM states, $\Delta E=0.683$ eV/supercell. This is consistent with the experimental findings[41,42] that oxygen vacancies stabilize the FM behavior in Co-doped ZnO thin films and agrees with the previous theoretical predication[50] that electron carriers are required to achieve ferromagnetism in bulk $Zn_{1-x}Co_xO$. For $Zn_{0.929}Fe_{0.071}O$ and $Zn_{0.929}Ni_{0.071}O$ thin films, the AFM interaction is found to be greatly degraded as the energy difference ΔE changes from -0.823 to -0.094 eV and from -0.102 to -0.026 eV for Fe-doped and Ni-doped ZnO systems, respectively. To see if it might be possible to turn an AFM coupling into a FM one by increasing the vacancy concentration, we removed one more O atom close to the Fe or Ni atoms (forming-Zn-V_O-T-V_O-T-). The energy difference ΔE is found to be changed to 0.048 and 0.086 eV for the supercells of $Zn_{0.929}Fe_{0.071}O$ and $Zn_{0.929}Ni_{0.071}O$, respectively. This indicates that V_O is capable of changing an AFM coupling into a FM one in Fe-doped or Ni-doped ZnO thin films when the concentration of V_O reaches a certain value. The prediction of ferromagnetism in Ni-doped ZnO is consistent with the experimental finding[52] that increasing n-type carrier is one of the essential factors for the conversion of PM Ni^{2+} ZnO nanocrystals into FM DMSs.

We note that filling oxygen vacancies in $Zn_{0.929}T_{0.071}O$ (T=Fe, Co, and Ni) seems to degrade the magnetic moment of the DMS samples and the local moment on each T atom (see Table III for instance). The total moment of a $Zn_{52}Co_4O_{54}$ supercell (containing two oxygen vacancies) is found to be $9.24\mu_B$ while for a defect-free $Zn_{52}Co_4O_{56}$ supercell it is $12.00\mu_B$, and the moment on each Co is decreased by $0.27\mu_B$/Co. Creating a V_O close to Co atoms (-Co-V_O-Co-) [as shown in Fig. 4(a)] was expected to increase the magnetic moment of Co due to a reduction in the coordination number. However, the distance between the two Co atoms was found to be greatly reduced from 2.85 to 2.27 Å, and the bond length between Co and O was found to be slightly contracted after structural optimization. The two Co atoms form a dimer, as shown in Fig. 4(b). The bond-length contraction leads to a strong hybridization between the two Co atoms as well as the Co and O atoms (see the charge-density distribution in Fig. 5). The electron carriers (e_{donor}^-) partially transfer onto Co^{2+}. As compared to the defect-free case, the above two factors result in the decrease in magnetic moments of $2.034\mu_B$ on each Co and drive the FM coupling between the two Co atoms in the $Zn_{0.929}Co_{0.071}O$ supercell. Note that the coupling in a Co dimer in the gas phase is calculated to be FM with $2.00\mu_B$ on each Co atom and the bond length between them is 1.98 Å.

2. Effect of zinc vacancy

We then created a Zn vacancy (V_{Zn}) by removing a Zn atom at the nearest-neighbor site to a T atom (forming -V_{Zn}-O-T-) on the surface layer of both the top and bottom sides of the $Zn_{0.929}T_{0.071}O$ supercell along the $[1\bar{1}00]$ direction. Calculations were carried out the same way as described above for the systems containing V_O. It was found that the presence of V_{Zn} (hole carriers) causes ferromagnetism in $Zn_{0.929}Cr_{0.071}O$ and $Zn_{0.929}Mn_{0.071}O$ thin films (see Table III). The energy difference ΔE is found to be 0.089 and 0.065 eV compared to -0.094 and -0.601 eV with no Zn vacancies for $Zn_{52}Cr_4O_{54}$ and $Zn_{52}Mn_4O_{54}$ supercells, respectively. These energies are much larger than the thermal energy corresponding to room temperature. Therefore, the FM states are stable with respect to thermal fluctuation. Increasing the Mn-Mn distance to 3.534 Å results in an expansion of 27.5% as compared to that in the defect-free system. The average bond length between Mn and O on the surface layer expands to 1.921 Å from 1.907 Å when the V_{Zn} is introduced. In Fig. 6, we present the charge-density distribution in the surface layer of the defect-free $Zn_{0.929}Mn_{0.071}O$ thin film and compare it with that in the system containing the Zn vacancy. We note that there is some overlap between charge densities on Zn and O, or Mn and O sites indicating that the bonding is covalent. However, when V_{Zn} is generated, i.e., hole carriers are introduced to the system, the charge-density distribution and the atomic positions of the Mn and O close to V_{Zn} are changed as shown in Fig. 6(b). Holes partially delocalize onto Mn^{2+}, which gives rise to Mn $3d$ level at the Fermi energy (see Fig. 7) and consequently ferromagnetism appears in the p-type Mn^{2+}:ZnO thin film, as suggested by experiments.[44]

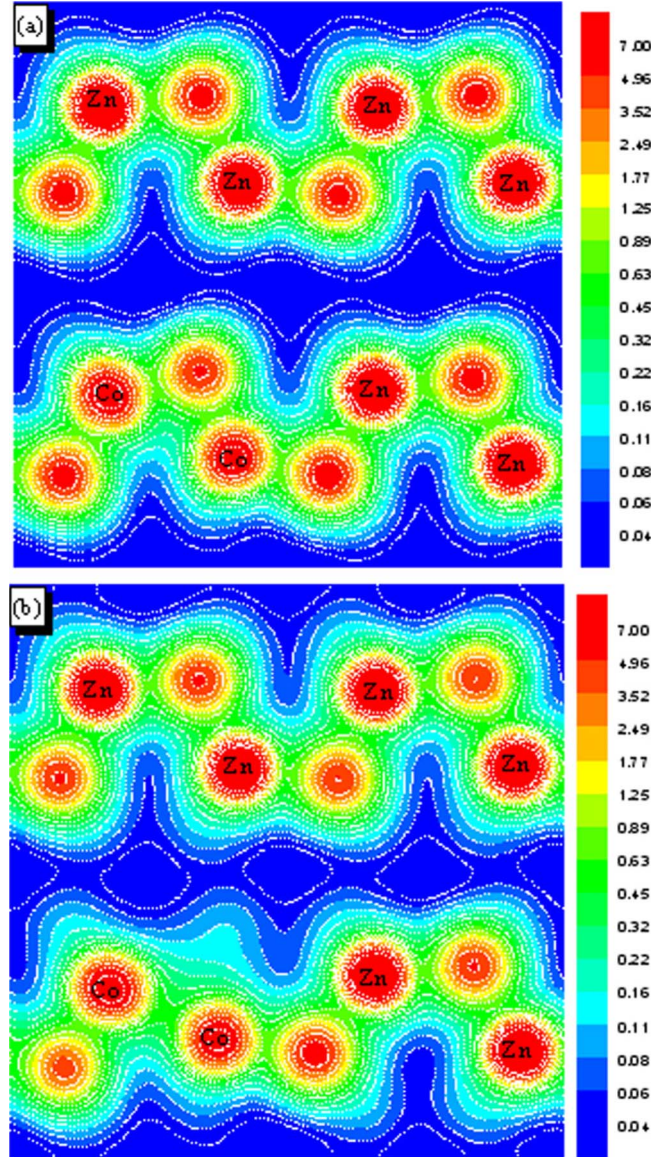FIG. 5. (Color online) Charge density distribution of (a) $Zn_{52}Co_4O_{56}$ and (b) $Zn_{50}Co_4O_{56}$ in the $[11\bar{2}0]$ plane of the surface layer.

For Fe-doped ZnO, introducing Zn vacancies makes the system FM. Although we note for both V_O and V_{Zn} that the nearest-neighbor Fe-Fe interaction becomes FM, the exchange coupling is much stronger for the system containing V_{Zn}. The FM state is found to be 0.887 eV lower in energy than the AFM state in $Zn_{50}Fe_4O_{56}$ (containing two Zn vacancies) while the FM state is only 0.086 eV lower in energy than the AFM state in $Zn_{52}Fe_4O_{54}$ (containing two O vacancies) (see Table III). Therefore, it is obvious that V_{Zn} (hole doping) is more effective in stabilizing ferromagnetism in Fe-doped ZnO than V_O (electron doping). Similar results were obtained in the experimental and theoretical studies on Fe-doped ZnO nanocrystals.[46] For Ni-doped ZnO, the Zn vacancy is also found to play a role in stabilizing the FM coupling as the FM state is found to become lower in energy than the AFM one as shown in Table III. However, the calculated results clearly show that the Zn vacancies in Co-
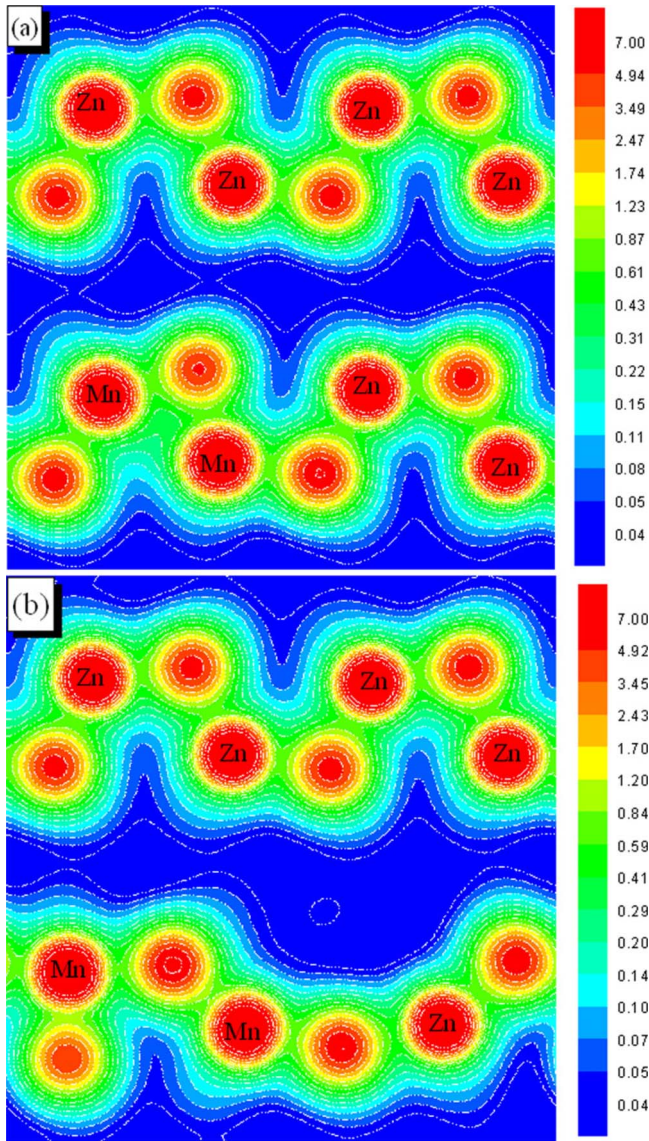
FIG. 6. (Color online) Charge density distribution of (a) $Zn_{52}Mn_4O_{56}$ and (b) $Zn_{50}Mn_4O_{56}$ in the $[11\bar{2}0]$ plane of the surface layer.

FIG. 7. (Color online) (a) Total DOS corresponding to $Zn_{52}Mn_4O_{56}$ supercell with and without V_{Zn}, (b) partial DOS of Mn $3d$, and (c) partial DOS of O $2p$ in $Zn_{52}Mn_4O_{56}$ with and without V_{Zn}.

doped ZnO favor antiferromagnetism and lead to a strong AFM interaction between the two Co ions. The energy difference ΔE is dramatically decreased from -0.098 to -0.501 eV when Zn vacancies are introduced in the $Zn_{0.929}Co_{0.071}O$ supercell.

3. Effect of oxygen and zinc interstitials

Since recent experiments have shown that Zn interstitials play an important role in development of ferromagnetism in Co-doped ZnO thin films, we have investigated how the interstitials influence the magnetic properties of Co-doped ZnO. For simulating both O and Zn interstitials in Co-doped ZnO, we considered two possible site locations: the hollow site (hs) and the bridge site (bs), as shown in Fig. 4(c). The hollow site is about ~ 0.9 Å above the surface layer, and has two Co, one Zn, and one O as the neighboring atoms. The bridge site is about ~ 1.23 Å above the surface, and has one
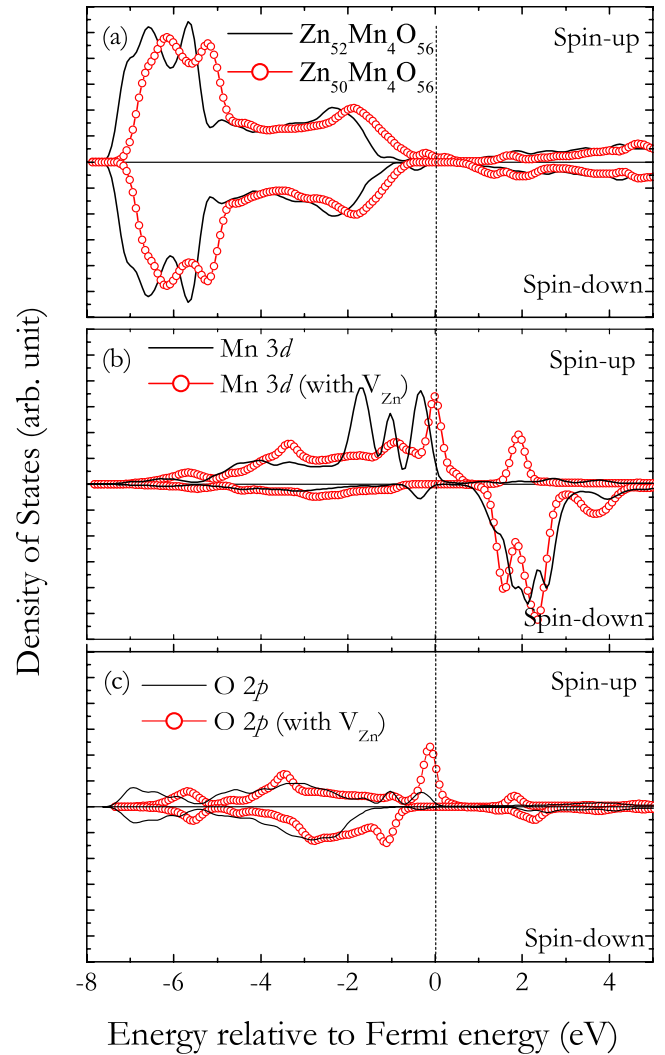
Co and one O as the nearest-neighbor atoms. Although it is known that there are two types of interstitial sites in bulk ZnO wurtzite structure and the energetically favorable site for a single Zn interstitial (Zn_i) is the octahedral site,[49] the distribution of defects in $Zn_xT_{1-x}O$ thin films is complicated.

It was found that O_i prefers to reside at the hollow site compared to the bridge site. In both configurations, adding two O atoms to the supercell further stabilizes the AFM state. For instance, the energy difference between the FM and AFM states ΔE decreases to -0.476 from -0.098 eV/supercell when two O atoms are introduced at the hollow site. The oxygen interstitials have little effects on the magnetic moments and the electronic structure of the Co-doped ZnO thin film. On the other hand, it was found that Zn_i prefers the bridge site over the hollow site. The coupling between the two Co atoms becomes FM and the energy difference ΔE changes from -0.098 to 0.205 eV/supercell, which is sufficient to overcome thermal fluctuations to provide robust FM behavior in the system. This agrees with the

TABLE IV. Total energy difference between the AFM and FM states ($\Delta E = E_{AFM} - E_{FM}$, in eV), total magnetic moment (μ_{total} in μ_B) per supercell, and local magnetic moment (μ_{Co} in μ_B) on each Co atom in $Zn_{52}Co_4O_{56}$ with the various defects.

$Zn_{52}Co_4O_{56}$	ΔE	μ_{total}	μ_{Co1}	μ_{Co2}
Defect-free	−0.098	0.000	2.309	−2.299
V_O	0.683	9.240	2.033	2.037
Zn_i	0.205	12.000	2.395	2.419
V_{Zn}	−0.501	0.022	2.457	−2.513
O_i	−0.476	0.033	2.328	−2.433

experimental findings[41–43] that Zn_i plays an important role in activating high-T_C ferromagnetism in Co^{2+}-doped ZnO. The relaxed geometry is given in Fig. 4(d). The distance between the Zn_i and the two Co atoms are 3.344 and 3.873 Å, respectively. The local magnetic moment on Co is increased by about $0.1\mu_B$.

The calculated total-energy difference ΔE and the magnetic moments for the ground-state configuration of $Zn_{52}Co_4O_{56}$ with and without the defects are tabulated in Table IV clearly showing that V_O and Zn_i turn the AFM coupling between Co atoms into FM. Moreover it stabilizes the FM coupling with a large energy difference $\Delta E = 0.683$ and 0.205 eV with the introduction of O vacancies and Zn interstitials, respectively. V_{Zn} and O_i favor AFM coupling and stabilize the AFM state by decreasing the energy difference ΔE from −0.098 eV to −0.581 and −0.476 eV when introducing V_{Zn} and O_i, respectively.

4. Vacancy distribution and concentration effect

To further verify the onset of ferromagnetism due to the vacancies and to study the effect of vacancy distribution and

concentration on the magnetic coupling, we have created V_{Zn} and O_i at different sites in the $Zn_{52}Co_4O_{56}$ supercell. We started with the ground-state configuration of $Zn_{52}Co_4O_{56}$ and created Zn vacancies at different sites on the surface and subsurface layers of the slab (see configurations C_{Z1}, C_{Z2}, and C_{Z3} in Fig. 8). Oxygen vacancies at difference sites, corresponding to configuration C_{11} to C_{22}, were then generated, as shown in Fig. 8. We studied the energetics of FM and AFM couplings between Co atoms for all these configurations. The calculated results are given in Table V.

The results clearly show that Zn vacancies stabilize the AFM coupling and lead to a strong AFM interaction between the two Co ions. The energy difference ΔE between the FM and AFM states changed from −0.098 to −0.501, −0.489, and −0.951 eV, respectively, for configurations C_{Z1}, C_{Z2}, and C_{Z3}. From the relative energy, we note that it costs less energy to generate a V_{Zn} close to a Co atom. When O vacancies are generated, on the other hand, the energy difference ΔE is considerably increased. For instance, the AFM coupling turns into the FM one with a large energy difference $\Delta E = 0.683$ eV/supercell in configuration C_{11}. For configurations C_{12}–C_{14}, ΔE increases from −0.098 eV to −0.034, −0.031, and −0.027 eV, respectively. The ground-state configuration was found to be configuration C_{13} that is still AFM, which indicates that it is easier to create a V_O further from Co atom. We, therefore, realized that a small concentration of V_O cannot lead to a transition from AFM to FM states, which has been confirmed by experiments.[41]

It is interesting to see that the FM state becomes much more stable than the AFM state for both configurations C_{21} and C_{22} in Fig. 8 when V_O concentration is increased to 7.14% by removing two O atoms on either side of the slab. The energy difference ΔE is 0.586 and 0.668 eV/supercell for C_{21} and C_{22}, respectively. This indicates that V_O is capable of tuning the magnetic coupling between Co atoms and
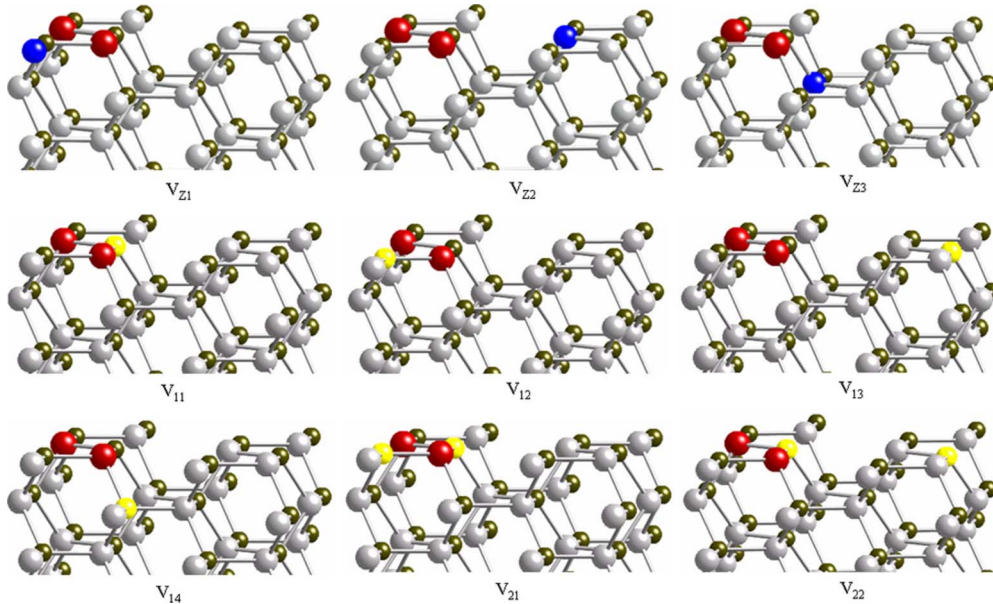

FIG. 8. (Color online) The schematic of the nonequivalent vacancy configurations in the ground state of $Zn_{52}Co_4O_{56}$ supercell (the lower part of the slab is removed). The lighter (bigger) spheres represent the Zn atoms, the darker (smaller) spheres represent the O atoms, and the red (biggest) spheres represent Co atoms. The blue and yellow spheres specify the sites where the atoms are removed to generate Zn and O vacancies, respectively.

TABLE V. Energy difference ΔE between AFM and FM states ($\Delta E = E_{AFM} - E_{FM}$, in eV/supercell), the relative energy $\Delta \varepsilon$ (in eV) calculated with respect to the ground state for each concentration of vacancies, optimized Co-Co distance $d_{Co1-Co2}$ and the average Co-O bond length d_{Co-O} (in Å), and the average magnetic moments (in μ_B) on Co atom for $Zn_{52}Co_4O_{56}$ supercell with and without defects. The first column specifies the defect configurations, as shown in Fig. 8, as well as defect concentrations.

Configurations	ΔE	$\Delta \varepsilon$	$d_{Co1-Co2}$	d_{Co-O}	M_{Co}
Without defects	−0.098		2.852	1.864	2.304
C_{Z1} (V_{Zn} at 3.57%)	−0.501	0.000	3.120	1.807	2.385
C_{Z2} (V_{Zn} at 3.57%)	−0.489	1.589	3.034	1.815	2.457
C_{Z3} (V_{Zn} at 3.57%)	−0.951	0.996	2.759	1.802	2.403
C_{11} (V_O at 3.57%)	0.586	0.580	2.270	1.892	2.084
C_{12} (V_O at 3.57%)	−0.034	0.541	2.659	1.862	2.058
C_{13} (V_O at 3.57%)	−0.031	0.000	2.776	1.868	2.269
C_{14} (V_O at 3.57%)	−0.027	1.652	3.108	1.852	2.206
C_{21} (V_O at 7.14%)	0.683	0.875	2.264	1.904	2.071
C_{22} (V_O at 7.14%)	0.668	0.000	2.259	1.898	2.075

stabilizing ferromagnetism in Co-doped ZnO when the concentration of V_O reaches a certain value. We note that configuration C_{22} is lower in energy by 0.873 eV than configuration C_{21}, demonstrating that V_O prefers to distribute uniformly in ZnO thin films.

The calculated total spin DOS and the partial DOS of Co 3d and O 2p for the ground state of configuration C_{22} in Fig. 8 are plotted in Figs. 9(a)–9(c), respectively. We see a significant change in the DOS around the Fermi level when O vacancies are introduced. The total DOS for spin up and spin down are not identical anymore, indicating that there is a moment in the system. The Fermi level with V_O present slightly moves to a higher energy range compared to that for $Zn_{52}Co_4O_{56}$. The main effect of V_O on the DOS, shown in Fig. 9(b), is a downward shift of the Co 3d spin-up states and an upward shift of the spin-down states, and there is a new peak appearing at 1.24 eV above the Fermi level in spin-up DOS. These show that the O vacancies have introduced new states in the gap region, resulting in FM coupling. This is due to the fact that Co atoms in $Zn_{1-x}Co_xO$ thin films behave as Co^{2+} (d^5). The Co^{2+} can readily substitute the group II cation, Zn, without the formation of structural defects or the generation of carriers. When a V_O is generated while two more electron carriers are introduced into the system. O vacancies which are known as shallow level donors can supply s and p spin carriers, and doped Co can supply local moments (spins). The s and p electrons partially delocalize onto Co^{2+}, and couple to the local spins via a FM s, p-d exchange interaction. The Zeeman splitting of the hopping s and p carriers in a modest field can be comparable to the thermal energy (k_BT), which gives rise to the new states of Co 3d and, consequently, to the FM coupling in the n-type Co^{2+}:ZnO thin films. Figures 9(b) and 9(c) show that the hybridization between Co 3d and O 2p at Fermi level becomes stronger when the O vacancies are introduced. Our finding is consistent with the previous theoretical prediction that sufficient electron carriers are required to achieve ferromagnetism in *bulk* $Zn_{1-x}Co_xO$,[50] while it is in contrast to some other DFT-based predictions where both hole doping

and electron doping promote FM in ZnO:Co and ZnO:Mn.[51] Recent experiments show that oxygen vacancies make ZnO:Co FM,[41,42,53] supporting our finding.

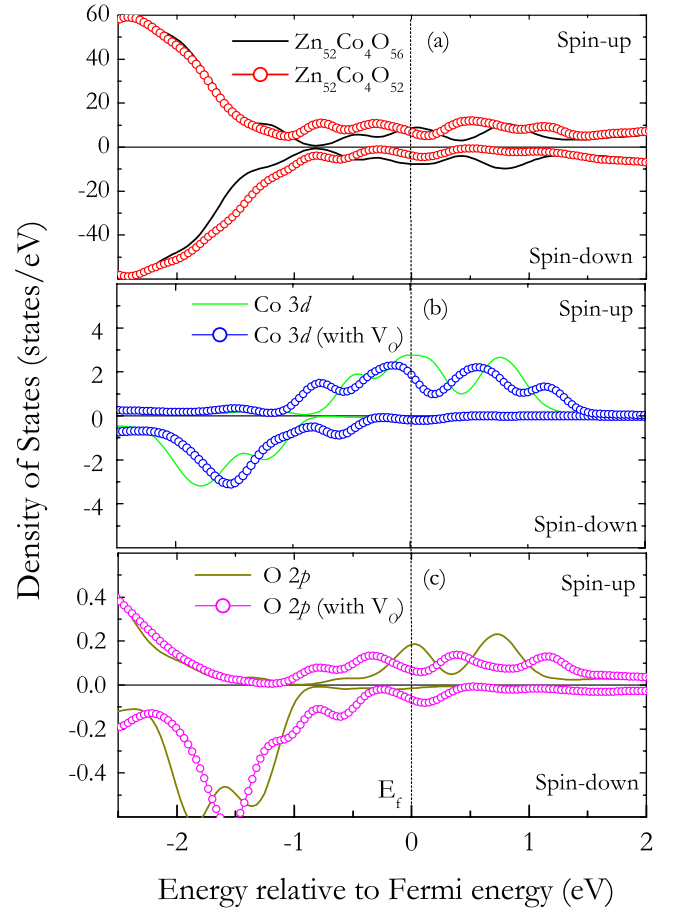Based on this study, one can expect that FM $Zn_{1-x}T_xO$ (T=Cr, Mn, Fe, Co, and Ni) thin films can be achieved de-

FIG. 9. (Color online) [(a)–(c)] Total spin DOS and partial spin DOS of Co 3d and O 2p orbitals corresponding to $Zn_{52}Co_4O_{56}$ supercell with and without the oxygen vacancies.

pending on the type and concentration of defects: the presence of *n*-type defects such as V_O and Zn_i causes magnetic interactions to remain AFM in $Zn_{1-x}T_xO$ (T=Cr and Mn) thin films, whereas *p*-type defects such as V_{Zn} and N substitution of O,[22,23] favor FM coupling, as observed. V_{Zn} is more effective in stabilizing ferromagnetism in $Zn_{1-x}T_xO$ (T=Fe and Ni). However, for Co-doped ZnO, there is a reverse correlation: Zn_i and V_O are the defects responsible for ferromagnetism. The possible reasons for this contrasting behavior are complicated as magnetic properties are influenced by many factors such as band gaps, the occupancy of the gap level, the symmetry of the energy level, crystal-field resonance, and dangling-bond hybrid, as discussed by Mahadevan and Zunger[54] in their systematic study of the magnetic properties of bulk GaAs doped with V, Cr, Mn, Fe, Co, and Ni. Magnetic properties are also known to be very sensitive to the local bonding environment. In the present case, thin-film geometry and the presence of vacancies and interstitials bring additional complexities such as reduction in the coordination number on the surface, bond-length contraction in and near the surface, and structure reconstruction caused by vacancies and interstitials.

We should also point out some intrinsic problems in the density-functional theory. It not only underestimates the energy-band gap but also predicts the impurity state of T $3d$ with some errors. Although Hubbard-U corrections[55] to local-density approximation or GGA can improve the description of the T d states in magnetic semiconductors, these corrections are generally not sufficient to open the band gap and remove spurious hybridization of the $3d$ orbitals with the host conduction band. Recently Lany *et al.*[56] have developed a "nonlocal external potential" method to overcome these difficulties. They found that electron doping is necessary to achieve ferromagnetism in the Co-ZnO system. This is in agreement with our finding that ferromagnetism is induced by Zn interstitials and oxygen vacancies. Moreover, the magnetic coupling between TM dopants is also dependent on their charge states.[57] The situation in thin films is more complex than that in the bulk since the bonding environments of TM dopants vary from the surface layer to the subsurface and inner layers due to different coordination number and different bond-length contraction. The presence of vacancies and interstitial atoms complicates the problem even further. Although some experimental methods to determine the charge state of T dopants[58] are available, accurate calculations of the charge state using DFT is difficult due to problems associated with the artificial use of the Wigner-Seitz cell for the computation of charge.

IV. SUMMARY

The electronic structure and magnetic properties of $Zn_{1-x}T_xO$ (T=Cr, Mn, Fe, Co, and Ni) ($11\bar{2}0$) thin films have been investigated systematically using first-principles calculations based on the gradient corrected density-functional theory and the supercell slab model. The main conclusions are: (1) the Cr, Fe, Co, and Ni dopants prefer to occupy surface sites instead of the bulk sites while Mn exhibits no site preference in the dilute regime and distributes uniformly in ZnO thin films; (2) $Zn_{1-x}T_xO$ ($11\bar{2}0$) thin film is intrinsically AFM because T^{2+} substitution at Zn sites in ZnO does not introduce any extra carriers. The AFM coupling is found to be insensitive to the concentration of dopants (from 7.14% to 14.29%) as observed by changing slab thickness from 7 to 11 layers along the $[11\bar{2}0]$ direction and from (1×2) to (2×2) along the $[1\bar{1}00]$ direction; (3) the magnetic coupling between T dopants, however, can be tuned by introducing native structural defects. Particularly, *p*-type defects, e.g., Zn vacancies, are necessary to change AFM coupling to FM in $Zn_{1-x}T_xO$ thin films (T=Cr, Mn, Fe, and Ni) depending on the defect concentration while *n*-type defects, e.g., O vacancy or Zn interstitial, are required to introduce FM coupling in $Zn_{1-x}Co_xO$ thin films. The interaction between the localized spins on the Co ions and delocalized carrier electrons originating from the O vacancies is responsible for the magnetic transition. Instead of clustering, V_O distributes homogenously on the surface of $Zn_{1-x}Co_xO$ thin films. Therefore, experimental conditions play a crucial role in observed magnetism, as native structural defects may be introduced during sample preparation. The present study provides a general picture of the magnetic properties of T-doped ZnO thin films and a different insight to understand the numerous conflicting experimental observations in T-doped ZnO systems.

*wangqian@swu.edu.cn

[1] T. Dietl, H. Ohno, F. Matsukura, J. Cibert, and D. Ferrant, Science **287**, 1019 (2000).

[2] S. W. Jung, S.-J. An, Gyu-Chul Yi, C. U. Jung, Sung-Ik Lee, and S. Cho, Appl. Phys. Lett. **80**, 4561 (2002).

[3] M. Venkatesan, C. B. Fitzgerald, J. G. Lunney, and J. M. D. Coey, Phys. Rev. Lett. **93**, 177206 (2004).

[4] Nick S. Norberg, K. R. Kittilstved, J. E. Amonette, R. K. Kukkadapu, D. A. Schwartz, and D. R. Gamelin, J. Am. Chem. Soc. **126**, 9387 (2004).

[5] J. R. Neal, A. J. Behan, R. M. Ibrahim, H. J. Blythe, M. Ziese, A. M. Fox, and G. A. Gehring, Phys. Rev. Lett. **96**, 197208 (2006).

[6] S. Kolesnik, B. Dabrowski, and J. Mais, J. Appl. Phys. **95**, 2582 (2004).

[7] O. D. Jayakumar, I. K. Gopalakrishnan, and S. K. Kulshreshtha, J. Mater. Sci. **41**, 4706 (2006).

[8] G. Lawes, A. S. Risbud, A. P. Ramirez, and R. Seshadri, Phys. Rev. B **71**, 045201 (2005).

[9] C. N. R. Rao and F. L. Deepak, J. Mater. Chem. **15**, 573 (2005).

[10] T. Shi, Sanyuan Zhu, Zhihu Sun, Shiqiang Wei, and Wenhan Liu, Appl. Phys. Lett. **90**, 102108 (2007).

[11] Z. Yin, N. Chen, F. Yang, S. Song, C. Chai, J. Zhong, H. Qian, and K. Ibrahim, Solid State Commun. **135**, 430 (2005).

[12] K. Ueda, H. Tabata, and T. Kawai, Appl. Phys. Lett. **79**, 988 (2001).

[13] Z. Jin, T. Fukumura, M. Kawasaki, K. Ando, H. Saito, T. Sekiguchi, Y. Z. Yoo, M. Murakami, Y. Matsumoto, T. Hasegawa, and H. Koinuma, Appl. Phys. Lett. **78**, 3824 (2001).

[14] T. Fukumura, Zhengwu Jin, M. Kawasaki, T. Shono, T. Hasegawa, S. Koshihara, and H. Koinuma, Appl. Phys. Lett. **78**, 958 (2001).

[15] A. S. Risbud, N. A. Spaldin, Z. Q. Chen, S. Stemmer, and R. Seshadri, Phys. Rev. B **68**, 205202 (2003).

[16] Ü. Özgür, Ya. I. Alivov, C. Liu, A. Teke, M. A. Reshchikov, S. Doğan, V. Avrutin, S.-J. Cho, and H. Morkoç, J. Appl. Phys. **98**, 041301 (2005).

[17] X. X. Wei, C. Song, K. W. Geng, F. Zeng, B. He, and F. Pan, J. Phys.: Condens. Matter **18**, 7471 (2006).

[18] H.-J. Lee, S.-Y. Jeong, C. R. Cho, and C. H. Park, Appl. Phys. Lett. **81**, 4020 (2002).

[19] W. Prellier, A. Fouchet, B. Mercey, Ch. Simon, and B. Raveau, Appl. Phys. Lett. **82**, 3490 (2003).

[20] D. A. Schwartz, K. R. Kittilstved, and D. R. Gamelin, Appl. Phys. Lett. **85**, 1395 (2004).

[21] S. Q. Zhou, K. Potzger, G. Talut, H. Reuther, J. von Borany, R. Grötzschel, W. Skorupa, M. Helm, J. Fassbender, N. Volbers, M. Lorenz, and T. Herrmannsdörfer, J. Appl. Phys. **103**, 023902 (2008).

[22] K. Sato and H. K. Yoshida, Semicond. Sci. Technol. **17**, 367 (2002).

[23] Q. Wang, Q. Sun, P. Jena, and Y. Kawazoe, Phys. Rev. B **70**, 052408 (2004).

[24] M. H. F. Sluiter, Y. Kawazoe, P. Sharma, A. Inoue, A. R. Raju, C. Rout, and U. V. Waghmare, Phys. Rev. Lett. **94**, 187204 (2005).

[25] A. Kaminski and S. Das Sarma, Phys. Rev. Lett. **88**, 247202 (2002).

[26] J. M. D. Coey, M. Venkatesan, and C. B. Fitzgerald, Nature Mater. **4**, 173 (2005).

[27] Q. Wang and P. Jena, Appl. Phys. Lett. **84**, 4170 (2004).

[28] Q. Wang, Q. Sun, P. Jena, and Y. Kawazoe, Appl. Phys. Lett. **87**, 162509 (2005).

[29] Q. Wang, Q. Sun, P. Jena, Z. Hu, R. Note, and Y. Kawazoe, Appl. Phys. Lett. **91**, 063116 (2007).

[30] W. Kohn and L. J. Sham, Phys. Rev. **140**, A1133 (1965).

[31] Y. Wang and J. P. Perdew, Phys. Rev. B **44**, 13298 (1991).

[32] G. Kresse and D. Joubert, Phys. Rev. B **59**, 1758 (1999).

[33] G. Kresse and J. Furthmüller, Phys. Rev. B **54**, 11169 (1996).

[34] R. W. G. Wyckoff, *Crystal Structures*, 2nd ed. (Wiley, New York, 1986), Vol. 1, p. 112.

[35] H. J. Monkhorst and J. D. Pack, Phys. Rev. B **13**, 5188 (1976).

[36] S. Yanagisawa, T. Tsuneda, and K. Hirao, J. Chem. Phys. **112**, 545 (2000).

[37] Q. Wang, Q. Sun, P. Jena, J. Z. Yu, R. Note, and Y. Kawazoe, Phys. Rev. B **72**, 045435 (2005).

[38] K. R. Kittilstved, D. A. Schwartz, A. C. Tuan, S. M. Heald, S. A. Chambers, and D. R. Gamelin, Phys. Rev. Lett. **97**, 037203 (2006).

[39] D. A. Schwartz and D. R. Gamelin, Adv. Mater. (Weinheim, Ger.) **16**, 2115 (2004).

[40] Judith L. MacManus-Driscoll, N. Khare, Y. L. Liu, and M. E. Vickers, Adv. Mater. (Weinheim, Ger.) **19**, 2925 (2007).

[41] E. Biegger, M. Fonin, U. Rüdiger, N. Janßen, M. Beyer, T. Thomay, R. Bratschitsch, and Y. S. Dedkov, J. Appl. Phys. **101**, 073904 (2007).

[42] C. Sudakar, P. Kharel, G. Lawes, R. Suryanarayanan, R. Naik, and V. M. Naik, J. Phys.: Condens. Matter **19**, 026212 (2007).

[43] N. H. Hong, J. Sakai, N. T. Huong, N. Poirot, and A. Ruyter, Phys. Rev. B **72**, 045336 (2005).

[44] W. Yan, Z. Sun, Q. Liu, Z. Li, Z. Pan, J. Wang, S. Wei, D. Wang, Y. Zhou, and X. Zhang, Appl. Phys. Lett. **91**, 062113 (2007).

[45] G. Weyer, H. P. Gunnlaugsson, R. Mantovan, M. Fanciulli, D. Naidoo, K. Bharuth-Ram, and T. Agne, J. Appl. Phys. **102**, 113915 (2007).

[46] D. Karmakar, S. K. Mandal, R. M. Kadam, P. L. Paulose, A. K. Rajarajan, T. K. Nath, A. K. Das, I. Dasgupta, and G. P. Das, Phys. Rev. B **75**, 144404 (2007).

[47] N. H. Hong, J. Sakai, and V. Brizé, J. Phys.: Condens. Matter **19**, 036219 (2007).

[48] S. B. Zhang, S.-H. Wei, and Alex Zunger, Phys. Rev. B **63**, 075205 (2001).

[49] A. Janotti and C. G. Van de Walle, Phys. Rev. B **76**, 165202 (2007).

[50] E. C. Lee and K. J. Chang, Phys. Rev. B **69**, 085205 (2004).

[51] N. A. Spaldin, Phys. Rev. B **69**, 125201 (2004).

[52] P. V. Radovanovic and D. R. Gamelin, Phys. Rev. Lett. **91**, 157202 (2003).

[53] M. Gacic, G. Jakob, C. Herbort, H. Adrian, T. Tietze, S. Brück, and E. Goering, Phys. Rev. B **75**, 205206 (2007).

[54] P. Mahadevan and A. Zunger, Phys. Rev. B **69**, 115211 (2004).

[55] V. I. Anisimov, I. V. Solovyev, M. A. Korotin, M. T. Czyżyk, and G. A. Sawatzky, Phys. Rev. B **48**, 16929 (1993).

[56] S. Lany, H. Raebiger, and A. Zunger, Phys. Rev. B **77**, 241201(R) (2008).

[57] Y. Zhao, P. Mahadevan, and A. Zunger, J. Appl. Phys. **98**, 113901 (2005).

[58] J.-H. Guo, A. Gupta, P. Sharma, K. V. Rao, M. A. Marcus, C. L. Dong, J. M. O. Guillen, S. M. Butorin, M. Mattesini, P. A. Glans, K. E. Smith, C. L. Chang, and R. Ahuja, J. Phys.: Condens. Matter **19**, 172202 (2007).